Journal of Optics
https://doi.org/10.1007/s12596-025-02528-7

RESEARCH ARTICLE

Design and numerical analysis of 4-inputs all-optical XOR gate in optical waveguides

Kalyan Kumar Ghosh[1] · Haraprasad Mondal[1] · Himanshu Ranjan Das[2] · Bhargabjyoti Saikia[1] · Mohammad Soroosh[3] · Eshan Adibnia[4]

Received: 24 October 2024 / Accepted: 13 January 2025

Abstract
In this article, a novel design of a 4-input all-optical XOR logic gate based on the principle of linear optics has been proposed. To design the proposed device, two-dimensional (2D) rods in air photonic crystal (PC) structure (where rods are arranged in a triangular lattice) has been chosen. A 340 μm^2 structure is taken where the radius of the silicon rods and the lattice constant of the structure have been selected as 120 nm and 600 nm respectively. To control the phase of the propagating optical waves through the waveguides, 3 Π-phase shifters have been utilized within the waveguides. Plane-wave expansion (PWE) method and finite difference time domain (FDTD) algorithm have been utilized to analyze the energy band diagram of the basic structure and to observe the electric field propagation profile of the device respectively. However, in the absence of optical nonlinearity, the proposed XOR gate has the ability to function in low-power input signals and provides a high response time of 0.57 picoseconds and a data rate of 660 Gbps (in the worst-case scenario). Moreover, the on-off contrast ratio of the proposed device has also been measured as 14.84 dB. Owing to its simple structural design and high-performance metrics altogether proves the proposed device is suitable as a component of future optical arithmetic and logic units (ALUs).

Keywords Photonic crystal · Phase shifter · XOR gate · Optical devices · Light beam interference · Plane wave expansion

Introduction

Nowadays, photonics plays a vital role in overcoming the drawbacks of existing technology, in the field of data communication and high-speed computation. Moreover, this technology is extended in view of applications into several fields of engineering such as healthcare [1, 2], automobile [3, 4], marine [5, 6], aeronautical [7, 8], etc. However, high-speed data communication has been achieved by optical fiber, but the main drawback lies in the signal processing terminal, where signals are processed still in the electronic domain. Therefore, signal conversion from optical to

✉ Haraprasad Mondal
mandal.haraprasad@gmail.com

Kalyan Kumar Ghosh
kalyanghosh042@gmail.com

Himanshu Ranjan Das
das.himanshu69@gmail.com

Bhargabjyoti Saikia
bhargab@dibru.ac.in

Mohammad Soroosh
m.soroosh@scu.ac.ir

Eshan Adibnia
ehsan.adibnia@pgs.usb.ac.ir

[1] Dibrugarh University Institute of Engineering and Technology, Dibrugarh University, Assam, India

[2] Department of Electronics and Communication Engineering, School of Engineering, Central University of Karnataka, Kalaburagi 585367, Karnataka, India

[3] Department of Electrical Engineering, Shahid Chamran University of Ahvaz, Ahvaz, Iran

[4] Faculty of Electrical and Computer Engineering, University of Sistan and Baluchestan (USB), P.O. Box 9816745563, Zahedan, Iran

Published online: 29 January 2025

electrical and vice versa (which limits the data processing speed and incurs high loss) is required at the interface between the optical fiber and signal processing terminal. To overcome these limitations, a group of researchers are motivated to design optical signal processing nodes [9–11]. As a result, a lot of research works in designing optical switches [12] and logic devices [13] have been published in the last couple of decades. To design optical signal processing nodes, researchers have adopted various optical techniques such as semiconductor optical amplifier (SOA) [14], plasmonics [15–18], waveguides [19], photonic crystals [20, 21] (PCs), etc. Among these existing technologies, PCs are especially promising as a photonic technology for integrated circuits, making them a focal point of extensive research for high-speed computing and data processing applications. PC has shown its promising candidature in the field of photonics research due to its precious photonic band gap (PBG) [22] property. This property talks about the transmission and reflection characteristics of various optical waves of PC structures. With the knowledge of PBG, and incorporating line defects by removing or altering (Rods/Holes) within the PC structure, waveguides are created, which are used to mold the propagation of light waves and to design various optical devices/switches and logic gates. In the last couple of decades, an enormous number of PC-based all-optical devices like decoders [23], multiplexers [24], adders [25], subtractors [26], logic gates [27, 28], etc. have been reported. These devices utilize the distinct characteristics of photonic crystals to manipulate and control light, paving the way for advanced solutions in high-speed data processing and computation.

However, to perform addition in binary arithmetic, subtraction/comparison operation, error detection and correction, etc. all-optical logic XOR gate is vital for designing optical arithmetic and logic units (ALUs). The beauty of the XOR gate is that, it can be integrated with other fundamental gates to execute complex operations, optimizing both the circuit's size and power efficiency. Moreover, in the recent past, several research articles for designing PC-based all-optical XOR logic gates have been published. For example, Sandip et al. [29] have reported a two-input optical XOR gate on a 2D-PC structure. In their work, 3 ring resonators and one reference input have been utilized to make the device function as an optical XOR gate. Their device offers a contrast ratio of 8.37 dB and provides 55% and 8% of input signal power (in the worst-case scenario) to the output port for establishing logic-1 and logic-0 respectively. Similarly, Ahmad and Saeed [30] have designed a two-input all-optical XOR gate in a 2D-PC structure by utilizing a nano-resonator. Optical beam interference phenomena is the main working principle of their device. The ON-OFF contrast ratio of their device is reported as 19.28 dB. Based on the optical beam interference method, another XOR gate has been designed by Kordi et al. [31]. A nano resonator has been incorporated by adding 3 rods (with different refractive indices) in the junction of the waveguides. The response time and contrast ratio of their device have been reported as 0.14 picoseconds and 15 dB respectively. In compression with [30, 31], Rao et al. [32] have presented an optical XOR gate (T-shaped) in 2D-PC, where the light beam interference method is a basic principle of operation. By removing rods in Γ-X direction, two input waveguides, one output waveguide, and one reference waveguide have been created and placed in such a way that it creates two junctions. Corner rods of the junctions and lengths of the waveguides (inputs and reference) have been optimized in such a way that the device can function as an XOR gate. The contrast ratio between the output logic levels ('1' and '0') has found as 8.29 dB. Moreover, Kouddad et al. [33] have reported an optical XOR gate (two-input) based on a resonant cavity and light beam interference principle. When one of the inputs is excited then 87% or 88% (01 and 10 input logic combinations respectively) of optical power reaches the output port. Again, when both the inputs are excited then due to destructive interference between signals no optical power reaches the output port, which satisfies the XOR logic operation. The contrast ratio, response time, and bit rate of their reported as 25.03 dB, 8.33 picoseconds, and 0.12 Tbit/s respectively. Furthermore, a two-input optical XOR gate has been designed on 42.24 μm^2 PC structure by Anagha and Jeyachitra [34]. The optical beam interference-based device demonstrates excellent performance, with a contrast ratio of 31.76 dB, a response time of 0.46 picoseconds, and a data rate of 2.12 Tbps. Moreover, Parandin and Alireza [35] have presented a PC-based optical XOR gate (two-input), where a machine learning algorithm has been used to optimize the performance of the device. At the junction of the device, a micro-cavity has been created by optimizing (using the K-Nearest Neighbors algorithm) the radius of four dielectric rods. With the help of micro-cavity and light beam interference principle, their two-input device functions as an optical XOR gate. Similar to [35], in [36] Shreya et al. have designed an XOR gate (T-shaped), where the radius of five dielectric rods (for micro-cavity at the junction) have been optimized. The insertion loss and response time of their device have been reported as -3.03 dB and 0.64 picoseconds respectively. On the other hand, by utilizing a non-linear directional coupler and light beam interference principle, Reyhaneh et al. [37] have designed a two-input XOR gate in a 2D-PC platform. 83% and 8% of input signal power reach the output port to establish logic-1 and logic-0 of the reported gate respectively. Studying previously published articles on all-optical logic XOR gates, it has been observed that most of the devices have two inputs

and they have been designed by using either a micro-cavity or micro-ring resonator which limits the operating bandwidth of the device. Moreover, due to fabrication tolerance if the length of the waveguides varies slightly then their devices' performance can be degraded.

Therefore, these limitations inspire the authors to develop an all-optical XOR gate with four inputs, operating within the linear optical principle where low optical power (absence of threshold power) is required to operate the device. Moreover, to the best of the authors' knowledge, none have devised a 4-input all-optical XOR logic gate till date. In this research, a 4-input all-optical XOR logic gate has been designed and the performance of the device has been analyzed. 2D PC, rods in air structure (where silicon rods are arranged in triangular lattice) has been used as the basic design platform of the proposed XOR gate. Using simple optical phenomena (constructive and destructive interference between optical waves) in the linear optical domain and maintaining a symmetrical shape, the proposed device has been designed. By removing rods in Γ-M direction four input waveguides and one output waveguide have been formed. Three Π-phase shifters within the input waveguides are embedded to create constructive or destructive operation between optical beams to make the device function as an XOR gate. The use of Π-phase shifters facilitates the symmetrical structure of the device. The incorporation of 2D-PC rods in air, along with the optimization of their parameters, showcases the potential for this projected device to be effectively integrated into practical photonic devices, with broad applications in photonics and optical communication systems.

However, this manuscript is prepared into four sections: Following the introduction section, the design process of the projected device and the energy band diagram of the structure have been discussed in detail in section two. Moreover, the propagation profile of the optical wave within the device and analysis of performance metrics like transmittance, contrast-ratio, and bit rate have been presented in the next section. In the same section, the three-dimensional (3-D) design and its electric field propagation profile have been discussed. In the final section, the conclusion of the work is written.

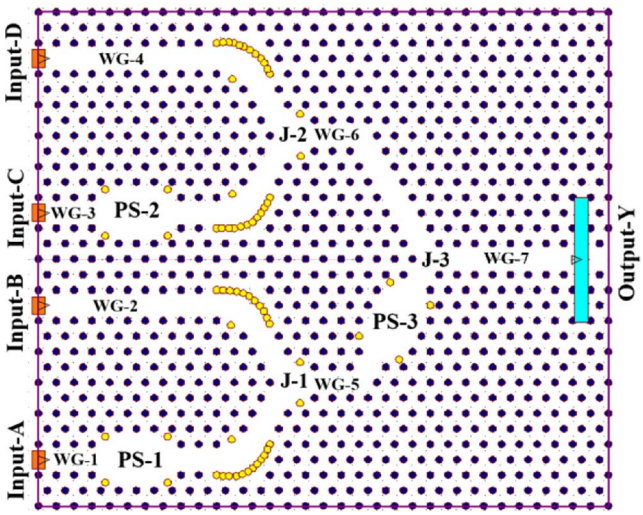

Fig. 1 Two-dimensional view of proposed 4-inputs XOR gate

Device design and band structure analysis

In this section, the detailed design procedure of the proposed optical XOR gate has been presented. For this design, a 2D-PC rods-in-air structure is utilized where a 33×33 array (in X-Z direction) of dielectric rods are arranged in a hexagonal lattice as shown in Fig. 1. Rods-in-air structures fundamentally offer a higher air-filling factor which marks in stronger photonic bandgap, enhancing the confinement and control of light within a certain range of frequencies. Moreover, in rods-in-air structures where the dielectric material is surrounded by an air background, leads to reduced scattering losses. Finally, the molding of light waves within the waveguides of rods-in-air structures is easy compared to holes-in-slab structures. However, the radius of the rods and the lattice constant of the structure have been selected as 120 nm and 600 nm respectively. The proposed device has four input ports (Input-A, Input-B, Input-C, and Input-D) and one output port (Output-Y) as presented in Fig. 1. One end of the waveguides, WG-1 and WG-2 (which are formed by introducing line defects through the alteration and removal of rods in the Γ-M direction) serve as Input-A and Input-B, respectively. These waveguides converge at junction J-1. Similarly, waveguides WG-3 and WG-4 are connected at one end to Input-C and Input-D, respectively, and their other ends merge at junction J-2. Additionally, waveguides WG-5 and WG-6 are each connected to junctions J-1 and J-2, respectively, with their opposite ends converging at junction J-3. Finally, waveguide, WG-7 connects junction, J-3 to the output port. Three Π-phase shifters [38] have been embedded in waveguides, WG-1, WG-1, and WG-3 to alter the phase of the optical signal by 180-degree. To implement a π-phase shifter within the waveguide, a W3 waveguide has been constructed in a specific segment by eliminating two additional rows of rods along the Γ-M direction over a length of three periods. Additionally, in the corner region of the W3 waveguide, four rods have been displaced by half a period towards the Γ-K direction, moving them away from the waveguide's center, as illustrated in Fig. 1. To improve the forward signal transmission and minimize back reflection (propagation loss) at the corner regions of the four waveguides (WG-1, WG-2, WG-3, and WG-4), twelve rods are strategically positioned at the outer sides of each corner,

overlapping with each other to smooth the corners. Additionally, the central rods located on the inner sides of each bend are shifted away from the waveguide's central axis (in the Γ-M direction) by half of the period.

Using the Plane Wave Expansion (PWE) algorithm [39] (implemented by MATLAB programming) the complete photonic energy band diagram for the non-defect PC structure has been computed across all directions of the irreducible Brillouin zone (Γ-M-K-Γ), as illustrated in Fig. 2a. Upon examining Fig. 2a, it is evident that the photonic band gap (PBG) is exclusively present in the transverse magnetic (TM) mode, spanning a normalized frequency range (a/λ) of 0.28 to 0.455. This range corresponds to specific wavelengths from 1320 nm to 2140 nm. Notably, the third optical window, as defined by the International Telecommunication Union (ITU) with a central wavelength of 1550 nm, lies within this normalized frequency range. Furthermore, Fig. 2a confirms that the proposed device operates most efficiently in the TM mode and lacks a band gap in the TE mode. Additionally, a W1 waveguide has been introduced along the Z-direction (Γ-M) of the crystal, and a projected band diagram has been generated using the PWE algorithm to analyze the frequency states within this waveguide, as illustrated in Fig. 2b. From the diagram, it is evident that there are no frequency states within the waveguide in the range of 0.28 to 0.345 (a/λ) (equivalent wavelength ranges between 1740 nm and 2140 nm). However, a distinct projected band is visible between 0.345 and 0.44 (a/λ) (equivalent wavelength ranges between 1360 nm and 1740 nm), indicating that waves can propagate through the waveguide in this normalized frequency range.

Results discussion and performance analysis

This section provides a detailed and insightful analysis of the results, evaluating the efficiency and effectiveness of the proposed device by measuring various performance metrics and comparing them with findings from other studies. To analyze the electric field propagation profile of the proposed device and to measure the performance metrics, the finite difference time domain (FDTD) algorithm [40] is used. To accurately compute the signal power distribution, the Perfectly Matched Layers (PML) absorbing boundary condition has been applied. A Gaussian optical monochromatic source emitting continuous wave (CW) (with a fixed power level of 1 μW/μm²) at a wavelength of 1550 nm is applied at each input port to evaluate the functionality of the proposed XOR gate. The optical intensity at the output is measured using a line monitor positioned at the output port. The spatial grid must be fine enough to ensure a comprehensive simulation, as determined by the signal's wavelength. For stability, the space-time grids should adhere to the specified equation, which is as follows:

$$c\Delta t = \frac{1}{\sqrt{\frac{1}{\Delta x^2} + \frac{1}{\Delta z^2}}} \tag{1}$$

Here, Δt represents the time step, c denotes the speed of light in free space, and Δx and Δz correspond to the spatial steps along the x- and z-axes, respectively.

However, the basic operating principle of the proposed device is light beam interference (constructive and destructive), which occurs at either junction, J-1 and J-2 or J-3. The designed XOR gate operates in sixteen unique states resulting from its four input variables, as shown in Table 1. Based on the interaction of the incoming light signals at the junctions, the output delivers either a high-intensity or low-intensity signal (representing logic-1 or logic-0 respectively). The truth table of the 4-input XOR gate, the initial phase of the signals applied at the input ports and the power level at the output port is depicted in Table 1.

Working function of optical XOR gate

The working function of the proposed device for all possible input logic combinations (sixteen) are explained in detail as follows:

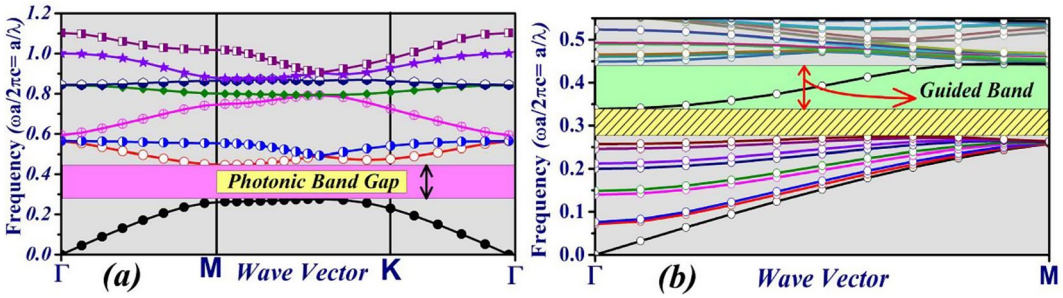

Fig. 2 (**a**) Complete photonic band diagram (**b**) Projected band diagram, of photonic crystal structure

Table 1 Truth table, initial phase of inputs and output power level of proposed optical XOR gate

Input logic level				Phase of input signals				Output logic level	Output power
I/P-A	**I/P-B**	**I/P-C**	**I/P-D**	**I/P-A**	**I/P-B**	**I/P-C**	**I/P-D**	**O/P-Y**	**O/P-Y**
0	0	0	0	0°	0°	0°	0°	0	$0P_i$
0	0	0	1	0°	0°	0°	0°	1	$0.61P_i$
0	0	1	0	0°	0°	0°	0°	1	$0.76P_i$
0	0	1	1	0°	0°	0°	0°	0	$0.01P_i$
0	1	0	0	0°	0°	0°	0°	1	$0.65P_i$
0	1	0	1	0°	0°	0°	0°	0	$0.003P_i$
0	1	1	0	0°	180°	0°	0°	0	$0.02P_i$
0	1	1	1	0°	0°	0°	0°	1	$0.63P_i$
1	0	0	0	0°	0°	0°	0°	1	$0.71P_i$
1	0	0	1	180°	0°	0°	0°	0	$0.002P_i$
1	0	1	0	0°	0°	0°	0°	0	$0.006P_i$
1	0	1	1	0°	0°	0°	0°	1	$0.7P_i$
1	1	0	0	0°	0°	0°	0°	0	$0.006P_i$
1	1	0	1	0°	0°	0°	0°	1	$0.72P_i$
1	1	1	0	0°	0°	0°	0°	1	$0.61P_i$
1	1	1	1	0°	0°	0°	0°	0	$0.003P_i$

Case-1 (Input combinations (ABCD) 0001, 0010, 0100, 1000)

When a continuous optical signal is applied to only one of the inputs, no interaction occurs between optical signals at the junctions since only one signal is present at any given time. Consequently, there is neither constructive nor destructive interference at the junctions. As a result, the input optical wave passes through to the output port with significantly high optical power (0001 = 0.61Pi, 0010 = 0.76Pi, 0100 = 0.65Pi, 1000 = 0.71Pi, where Pi is considered as input power), thereby establishing a logic-1 output condition. The electric field propagation profiles and time-evolving output power graphs are depicted in Figs. 3a/4a, 3b/4b, 3d/4d, and 3h/4h for input combinations 0001, 0010, 0100, and 1000 respectively.

Case-2 (Input combinations (ABCD) 0011, 1100)

When either the pair of inputs, Input-A and Input-B, or Input-C and Input-D are excited with an optical wave, destructive interference occurs due to the π-phase shifter, which alters the phase of the input signal by 180°. This interference happens at junction J-1 or J-2, depending on the input pairs, preventing any optical power from reaching the output port, thereby resulting in a logic-0 output condition (0011 = 0.01Pi and 1100 = 0.006Pi). The optical wave propagation profiles for these conditions are illustrated in Fig. 3c and l, while the time response and output power profiles are depicted in Fig. 4c and l for the input logic combinations 0011 and 1100, respectively.

Case-3 (Input combinations (ABCD) 0101)

When continuous optical waves are introduced at Input-B and Input-D, the signal at Input-B experiences a 180° phase shift due to the action of phase shifter PS-3. In contrast, the signal at Input-D passes through without encountering any phase shifter, so no 180° phase shift occurs. These optical signals then converge at junction J-3, where they interfere destructively due to being out of phase, as illustrated in Fig. 3e. As a result, almost no optical power (approximately 0.003) is detected at the device's output port, indicating a logic-0 output condition (the corresponding time response is shown in Fig. 4e).

Case-4 (Input combinations (ABCD) 0110)

In this case, the signal applied at Input-B is initially set with a phase of 180°, while another signal is simultaneously applied at Input-C. The presence of phase shifters, PS2 and PS3, causes these two signals to intersect at junction J-3 in opposite phases, leading to destructive interference at that point (as shown in Fig. 3f). As a result of this destructive interference, the power of both signals is effectively canceled out at junction J-3, thereby satisfying the output logic-0 condition with an output power of 0.02Pi.

Case-5 (Input combinations (ABCD) 0111, 1011, 1101, 1110)

In this scenario, three continuous optical signals are simultaneously applied to three input ports. This means that both inputs from one input pair (either Input-A and Input-B or Input-C and Input-D) are activated, while a single input from another pair is also excited. Destructive interference

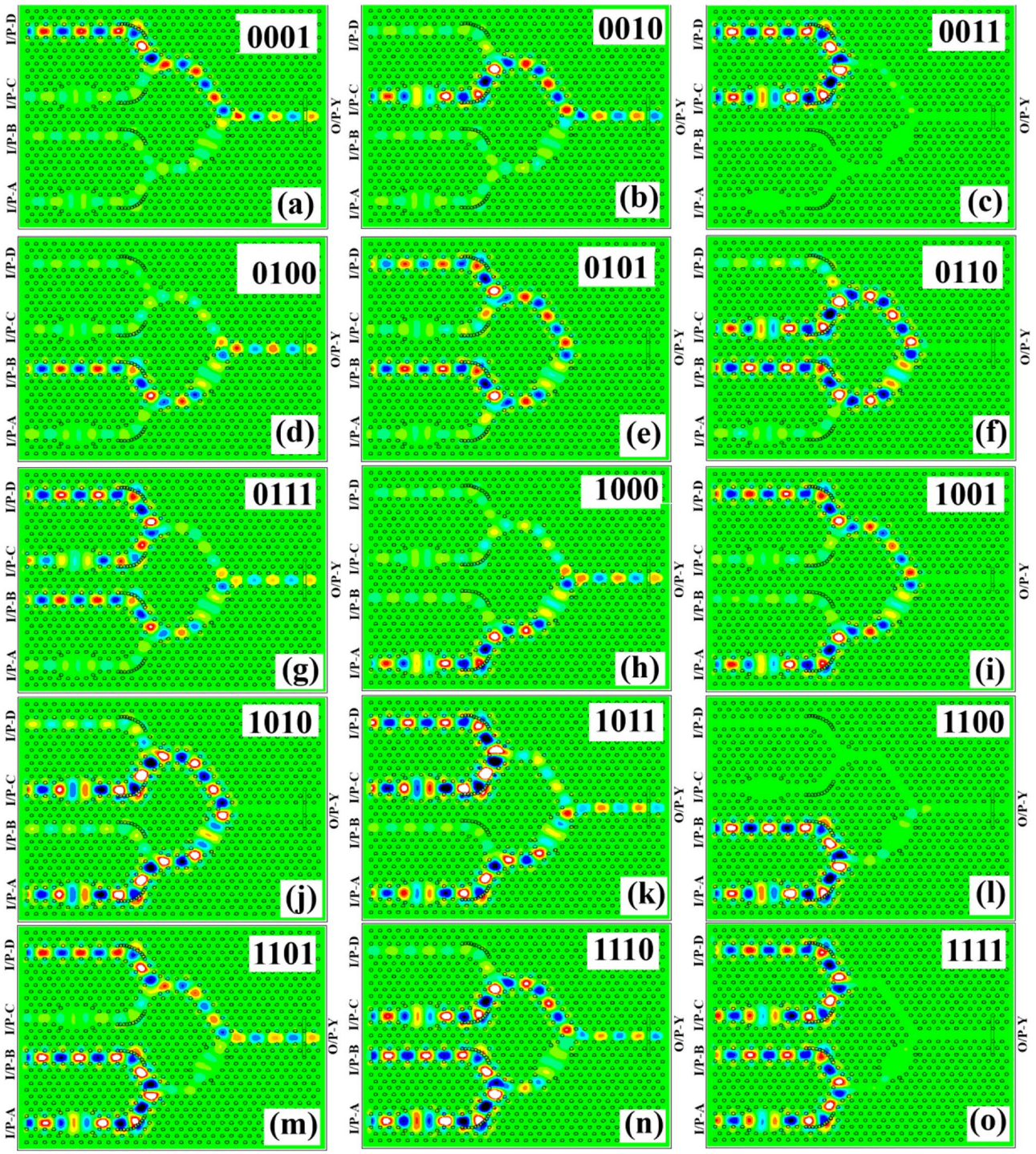

Fig. 3 Optical wave propagation profile (obtained from FDTD) for the input (ABCD) logic combination of (**a**) 0001 (**b**) 0010 (**c**) 0011 (**d**) 0100 (**e**) 0101 (**f**) 0110 (**g**) 0111 (**h**) 1000 (**i**) 1001 (**j**) 1010 (**k**) 1011 (**l**) 1100 (**m**) 1101 (**n**) 1110 (**o**) 1111

occurs at either junction J-1 or J-2 when both inputs from one pair are excited. Additionally, the power of the single excited input signal from the other pair for input combinations (0111, 1011, 1101, and 1110) does not participate in any interference operation. Instead, it reaches the output port with significantly high optical power, justifying the logic-1 output condition (0111 = 0.63Pi, 1011 = 0.7Pi, 1101 = 0.72Pi, and 1110 = 0.61Pi). The optical wave propagation profiles obtained from the FDTD simulation algorithm, along with the time response graphs, are shown for input logic combinations 0111, 1011, 1101, and 1110 in Figs. 3g/4g, 3k/4k, 3m/4m, and 3n/4n, respectively.

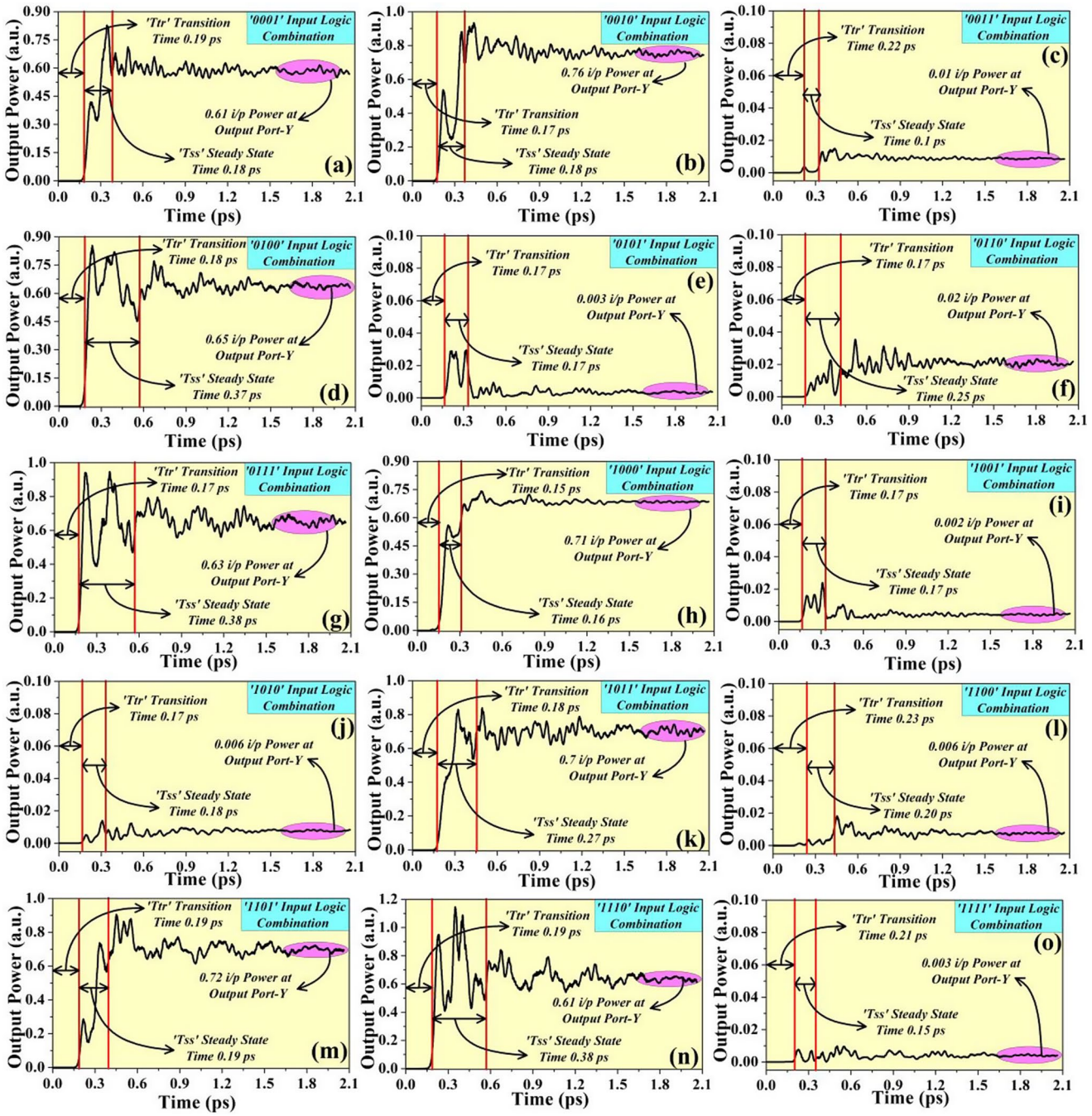

Fig. 4 Time evolving graph for the input (ABCD) logic combination of (**a**) 0001 (**b**) 0010 (**c**) 0011 (**d**) 0100 (**e**) 0101 (**f**) 0110 (**g**) 0111 (**h**) 1000 (**i**) 1001 (**j**) 1010 (**k**) 1011 (**l**) 1100 (**m**) 1101 (**n**) 1110 (**o**) 1111

Case-6 (Input combinations (ABCD) 1001)

Similar to case-4, here, the signal at Input-A is initially set with a 180° phase, while another signal is simultaneously introduced at Input-D. Due to the phase shifters, PS1 and PS3, these two signals converge at junction J-3 in opposite phases, resulting in destructive interference at that point (the signal propagation profile is illustrated in Fig. 3i, and the time response graph is shown in Fig. 4i). This destructive interference effectively cancels out the power of both signals at junction J-3, thereby ensuring the output logic-0 condition, with the extremely low output power of 0.002Pi.

Case-7 (Input combinations (ABCD) 1010)

When continuous optical waves are introduced at Input-A and Input-C, the signal at Input-A undergoes a 360° phase shift due to the combined effects of phase shifters PS-1 and PS-3. Meanwhile, the signal at Input-C experiences a 180° phase shift as it passes through phase shifter PS-2. These phase-altered signals converge at junction J-3, where they meet out of phase, leading to destructive interference, as depicted in Fig. 3j. Consequently, almost no optical power (approximately 0.006Pi) is detected at the device's output port, confirming the output logic-0 condition (the time response graph for this case is presented in Fig. 4j).

Case-8 (Input combinations (ABCD) 1111)

In this scenario, continuous Gaussian waves are applied to all input ports. At junction J-1, the optical signals from Input-A and Input-B interact, resulting in destructive interference. This occurs because the phase-shifter PS-1 introduces a 180° phase shift to the signal from Input-A. Similarly, at junction J-2, the signals from Input-C and Input-D also undergo destructive interference as described in figures-3o and 4o. Consequently, minimal optical power (0.003Pi) is detected at the output port, confirming the logic-0 output condition.

However, the figure of merit (FOM) for an optical XOR gate (PhC-based) is a crucial parameter that is used to evaluate the performance of the device. FOM of an XOR gate typically involves performance metrics like Contrast Ratio (CR), Bit Error Rate (BER), operating speed, power consumption, Insertion loss, footprint, crosstalk, bandwidth, etc. The contrast ratio is defined as a ratio between the minimum value of logic-1 power and the maximum value of logic-0 power in the output port. The higher value of the contrast ratio provides a lower probability of bit error hence low BER which signifies better reliability. Moreover, operating speed is defined by the device's response time which helps to calculate the bit rate of the device. Loss of optical power while propagating through the device is defined as insertion loss and its lower value is always preferable. However, the range of wavelengths where a device is capable of functioning effectively is known as bandwidth (BW) (wider BW is always desirable). In the following subsections, the performance matrices related to the FOM of the proposed XOR gate have been discussed in detail.

Response time and data rate

The response time of a device is an important factor that directly impacts its propagation delay and data transfer rate. The response time of a device is determined by measuring the time it takes for a signal to travel from the input port to the output port, achieving its maximum output power with steady state. This response time consists of two components: transition time (Ttr) and steady-state time (Tss). The time required for a signal to travel from the input to the output after initiation is called the transition time (Ttr). On the other hand, the steady-state time (Tss) refers to the time required for a signal to reach at least 90% of its stable value after the transient phase has passed. In this study, we have calculated the response time, transition time, and steady-state time of the proposed device under all possible input conditions, using time-evolution graphs. A total of sixteen simulations have been conducted to analyze the transition time (Ttr) and steady-state time (Tss) across various input signal combinations, as illustrated in Fig. 4. The corresponding values for transition time and steady-state time for each input combination are detailed in Table 2.

Based on Table 2, it is observed that the device's response time ranges from 0.31 ps to 0.57 ps. Notably, the minimum response time of 0.31 ps (transition time is 0.15 ps and steady-state time is 0.16 ps) occurs with the '1000' input logic combination, while the maximum response time of 0.57 ps (transition time is 0.19 ps and steady-state time is 0.38 ps) is recorded with the '1110' input logic combination. The steady-state time (Tss) of the response is a crucial parameter for determining the bandwidth and bit rate of the device. As illustrated in Fig. 4, the steady-state time is observed to be 0.38 picoseconds for the input logic '0111/1110' and 0.1 picoseconds for the input logic '0011' under the best and worst-case scenarios, respectively. Due to the operation in the linear optical domain, the signal's falling time is expected to match the rise time, with values of 0.38 picoseconds and 0.1 picoseconds corresponding to the input logic '0111/1110' and '0011', respectively. Thus, for a narrow pulse, the channel's bandwidth is calculated as 1/2Tss, resulting in a best-case scenario bandwidth of 5 THz. In non-return-to-zero (NRZ) systems, where a bit is represented by half of the cycle, the bit rate is determined by 1/2Tss. Conversely, in return-to-zero (RZ) systems, where a full cycle is used, the bit rate is calculated as 1/4Tss. Therefore, the proposed device supports a maximum bit rate of 5 Tbps for NRZ systems and 2.5 Tbps for RZ systems, summarized in Table 2. However, in the worst-case scenario, the device is capable of operating at a bit rate of approximately 660 Gbps.

Contrast ratio (CR) and return loss (RL)

Another key parameter for evaluating the performance of optical logic devices or switches is the contrast ratio, also known as the extinction ratio. This ratio, measured in decibels (dB), is determined by comparing the signal power at

Table 2 Response time, transition time, steady-state time, bandwidth, and bit rate of the proposed XOR gate

Inputs	Response Time (ps)	(Ttr) (ps)	(Tss) (ps)	Bandwidth (THz)	Bit Rate (Tb/s) RZ	Bit Rate (Tb/s) NRZ	Inputs	Response Time (ps)	(Ttr) (ps)	(Tss) (ps)	Bandwidth (THz)	Bit Rate (Tb/s) RZ	Bit Rate (Tb/s) NRZ
0000	-	-	-	-	-	-	**1000**	0.31	0.15	0.16	3.13	1.57	3.13
0001	0.37	0.19	0.18	2.78	1.39	2.78	**1001**	0.34	0.17	0.17	2.94	1.47	2.94
0010	0.35	0.17	0.18	2.78	1.39	2.78	**1010**	0.35	0.17	0.18	2.78	1.39	7.78
0011	0.32	0.22	0.10	5	2.5	5	**1011**	0.45	0.18	0.27	1.85	0.93	1.85
0100	0.55	0.18	0.37	1.35	0.675	1.35	**1100**	0.43	0.23	0.20	2.5	1.25	2.5
0101	0.34	0.17	0.17	2.94	1.47	2.94	**1101**	0.38	0.19	0.19	2.63	1.32	2.63
0110	0.43	0.17	0.25	2	1	2	**1110**	0.57	0.19	0.38	1.32	0.66	1.32
0111	0.55	0.17	0.38	1.32	0.66	1.32	**1111**	0.36	0.21	0.15	3.33	1.67	3.33

the output port when the device is in the logic-1 state to the signal power in the logic-0 state. Mathematically, the contrast ratio can be represented as:

$$CR = 10log_{10}\frac{P_1}{P_0} \tag{2}$$

Here, P1 and P0 represent the signal power levels at the output port for logic-1 and logic-0, respectively. Additionally, the contrast ratio is directly related to the noise margin and inversely related to the bit error rate (BER), which quantifies the number of bit errors occurring in a transmission system over a specified time period. The noise margin determines a device's tolerance to interference. A higher noise margin results in greater protection against noise. Additionally, a logic device with a high contrast ratio exhibits better noise immunity and a lower likelihood of bit errors. In our proposed device, the output power levels for all possible input combinations have been measured. From these measurements, 0.02Pi is determined to be the maximum value for logic-0 at the output port, while 0.61Pi is identified as the minimum value for logic-1. Using Eq. 2, the contrast ratio for the proposed XOR gate has been calculated, yielding an impressive result of 14.84 dB.

Return loss (RL) is a critical parameter for evaluating optical logic devices. It is determined by calculating the ratio between the light applied into the device and the light reflected back toward the source and it is measured in dB scale. Mathematically, return loss can be expressed as:

$$RL = 10log_{10}\frac{P_{in}}{P_{ret}} \tag{3}$$

Where, P_{in} represents the signal power applied at the input port, while P_{ret} denotes the power of the signal reflected back at the input port. A high return loss is desirable for optimal device performance, as it indicates better efficiency and minimal signal reflection [34]. The return losses for each input waveguide (WG-1, WG-2, WG-3, and WG-4) of the proposed device have been determined. To calculate the return loss for a specific waveguide, an optical source is positioned 4.8 μm away from the input port within the waveguide, while an optical detector is placed right at the beginning of the input port. Using Equation-3, the return losses for WG-1, WG-2, WG-3, and WG-4 have been found to be 6.57 dB 8.24dB, 6.57dB, and 8.24dB respectively.

Moreover, the insertion loss of the proposed device has also been calculated. The insertion loss of an optical device is a ratio between optical power received at the output port with the optical power is applied at the input port. For better performance of the device low insertion loss is desirable. Numerically, the contrast ratio is calculated as

$$Insertion\ Loss\ (IL) = -10log_{10}\frac{P_{out}}{P_{in}} \quad (4)$$

Where, P_{out} and P_{in} are considered as output and input power of the device respectively. When no interference phenomena is occurred in the junction (means only single input port is excited) then the output power is measured which helps to calculate the IL of the proposed device. For example, in 0001 input logic combination (only optical signal is applied at input A) 61% of input power is received at the output port which leads to insertion loss as 2.14 dB.

Transmittance

Transmittance is a crucial parameter in evaluating the performance of an optical device or logic gate. In our proposed device, the transmittance has been analyzed for four input logic combinations: 1111, 1011, 1000, and 0011 representing both logic 0 and logic 1 states at the output port. Transmittance is measured by obtaining the optical signal power at the output port for different input wavelengths. Figure 5a illustrates the transmittance for the input combination 1111, with the input signal wavelength varying from 1300 to 1700 nm. The minimum transmittance is observed at a wavelength of 1550 nm. Similarly, Fig. 5d illustrates the transmittance for the input combination 0011, with the input signal wavelength varying from 1300 to 1800 nm. The minimum transmittance is observed at a wavelength of 1550 nm. Additionally, the device demonstrates nearly zero output power within the 1540 to 1595 nm, wavelength range, indicating a bandwidth of approximately 6.5 THz. Similarly, the transmittance behavior for the input combination 1011, and 1000 are depicted in Fig. 5b and c respectively. The maximum transmittance of 0.7 is achieved at 1550 nm for both input logic combinations. The device also exhibits high transmittance within the 1537 to 1565 nm range, offering a bandwidth of about 3.5 THz cantered around 1550 nm. The above analysis confirms that the proposed device delivers excellent performance across a broad spectral range. These transmittance characteristics ensure that the XOR gate is capable of functioning efficiently across the entire C-band used in telecommunication systems.

Comparative study with existing work

A comprehensive analysis has been conducted by referencing the existing literature, as shown in Table 3. Table 3 reveals that all the reported works [29–37] utilize beam interference in combination with micro ring resonators, resonant cavities, or directional couplers. The studies [29–36] are grounded in the principles of linear optics, while the work in [37] explores non-linear materials, which inherently face challenges such as the need for high operating power and extended lengths for effective light-matter interaction. Furthermore, all-optical XOR gates with two inputs have been reported across [29–37]. In terms of response time, the shortest reported duration is 0.14 picoseconds in [31], while the longest is 8.33 picoseconds in [33]. Additionally, the highest contrast ratio of 118 dB and the fastest data rate of 2.17 Tbps are found in [35] and [34], respectively.

The proposed device is uniquely designed using a two-dimensional photonic crystal (PC) structure with rods in air. Unlike other designs, it relies solely on light beam interference, with no nonlinear components. To the best of the

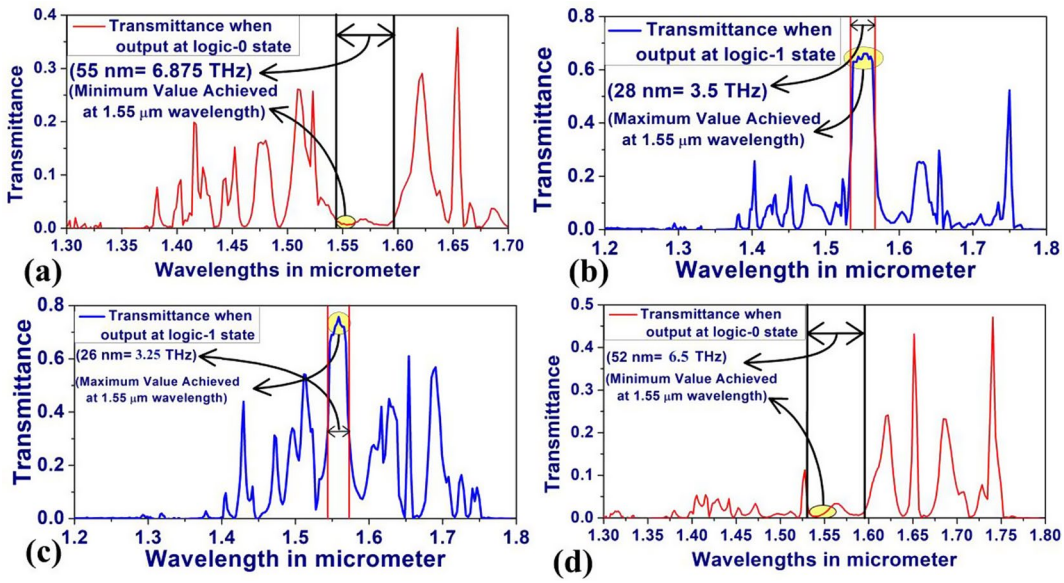

Fig. 5 Transmittance of proposed device at (**a**) logic-0 output condition (when inputs = 1111) (**b**) logic-1 output condition (when inputs = 1011) (**c**) logic-1 output condition (when inputs = 1000) (**d**) logic-0 output condition (when inputs = 0011)

Table 3 Comparative study with published articles

Ref.	Platform used	Operating principle	Foot-print (μm^2)	Response time (ps)	Contrast ratio (dB)	Data rate (Tbps)
[29]	Rods-in-air	Ring resonator based on linear optics. (2-inputs)	295	---	8.37	---
[30]	Rods-in-air	Nano ring resonator and beam interference in linear optics. (2-inputs)	252	0.466	19.95 (dB)	---
[31]	Rods-in-air	Microcavity and beam interference in linear optics. (2-inputs)	60.2	0.14	14.7	---
[32]	Rods-in-air	Beam interference in linear optics. (2-inputs)	45.36	---	8.29	---
[33]	Rods-in-air	Microcavity and beam interference in linear optics. (2-inputs)	75.71	8.33	25.03	0.12
[34]	Rods-in-air	Beam interference in linear optics. (2-inputs)	42.24	0.46	31.76	2.17
[35]	Rods-in-air	Microcavity and beam interference in linear optics. (2-inputs)	81	---	118	---
[36]	Rods-in-air	Microcavity and beam interference in linear optics. (2-inputs)	144	0.64	82.25	1.563
[37]	Rods-in-air	Directional coupler and beam interference in non-linear optics. (2-inputs)	843	1	---	---
This work	Rods-in-air	Beam interference in linear optics. (4-inputs)	340	0.31 = Best and 0.57 = Worst	14.84	0.66 = Worst 5 = Best

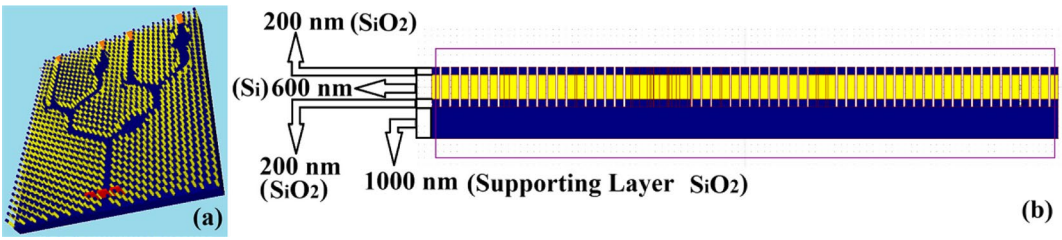

Fig. 6 (**a**) Three-dimensional view of proposed 4-inputs XOR gate, (**b**) Side view of the proposed structure

authors' knowledge, this is the first time a PC-based four-input optical XOR gate has been introduced. Despite incorporating four input ports and phase shifters within the input waveguides to maintain a symmetrical design, the device achieves a compact footprint of 340 μm². Additionally, the linear optical design ensures a high contrast ratio of approximately 15 dB and a data rate of 660 Gbps.

3-dimensional (3-D) design and fabrication feasibility

Any physical device must have finite dimensions in all three directions. Accordingly, the design procedure of the proposed optical gate has been discussed with a finite slab height of 2 μm. The 3-dimensional design of the device is illustrated in Fig. 6a, where the height of each rod is set to 1 μm. These rods are composed of three distinct layers: the top and bottom layers are 0.2 μm (200 nm) thick, while the middle layer measures 0.6 μm (600 nm), as shown in Fig. 6b. To ensure mechanical stability, the dielectric rods, suspended in an air background, rest on a supporting silica (SiO_2) layer with a thickness of 1 μm. For symmetry along the Y-axis, each rod is uniformly structured with these three layers (see Fig. 6b). Since the supporting layer is made of SiO_2, the top and bottom layers of the rods are also fabricated from SiO_2, while the middle layer—responsible for the propagation of optical waves—is composed of silicon (Si). The total height of the device is 2 μm, where 1 μm accounts for the supporting slab and the remaining 1 μm corresponds to the height of the rods (with 200 nm allocated to each top and bottom layer, and 600 nm to the middle propagating layer). The permittivity (ε) of the middle silicon layer is set to 11.9.

Furthermore, the CMOS fabrication process has matured significantly, making the production of this structure now achievable. While various methods exist for fabricating photonic crystal (PC) structures, the proposed multilayer 2D PhC rods-in-air design can be implemented using procedures similar to those outlined in [41–44]. The fabrication steps can be broadly summarized as follows:

- Preparation of the supporting layer (bottom layer), made of SiO_2 is done by the process of oxidation on silicon wafer.
- By the MBE (Molecular Beam Epitaxy)/ PECVD (Plasma-enhanced chemical vapor deposition) method Si layer (The middle layer where propagation takes place) is deposited on the SiO_2 layer.
- Sputter deposition of SiO_2 layer (top layer) on Si layer (middle layer).
- For patterning, the photoresist material is deposited on top of the prepared wafer.

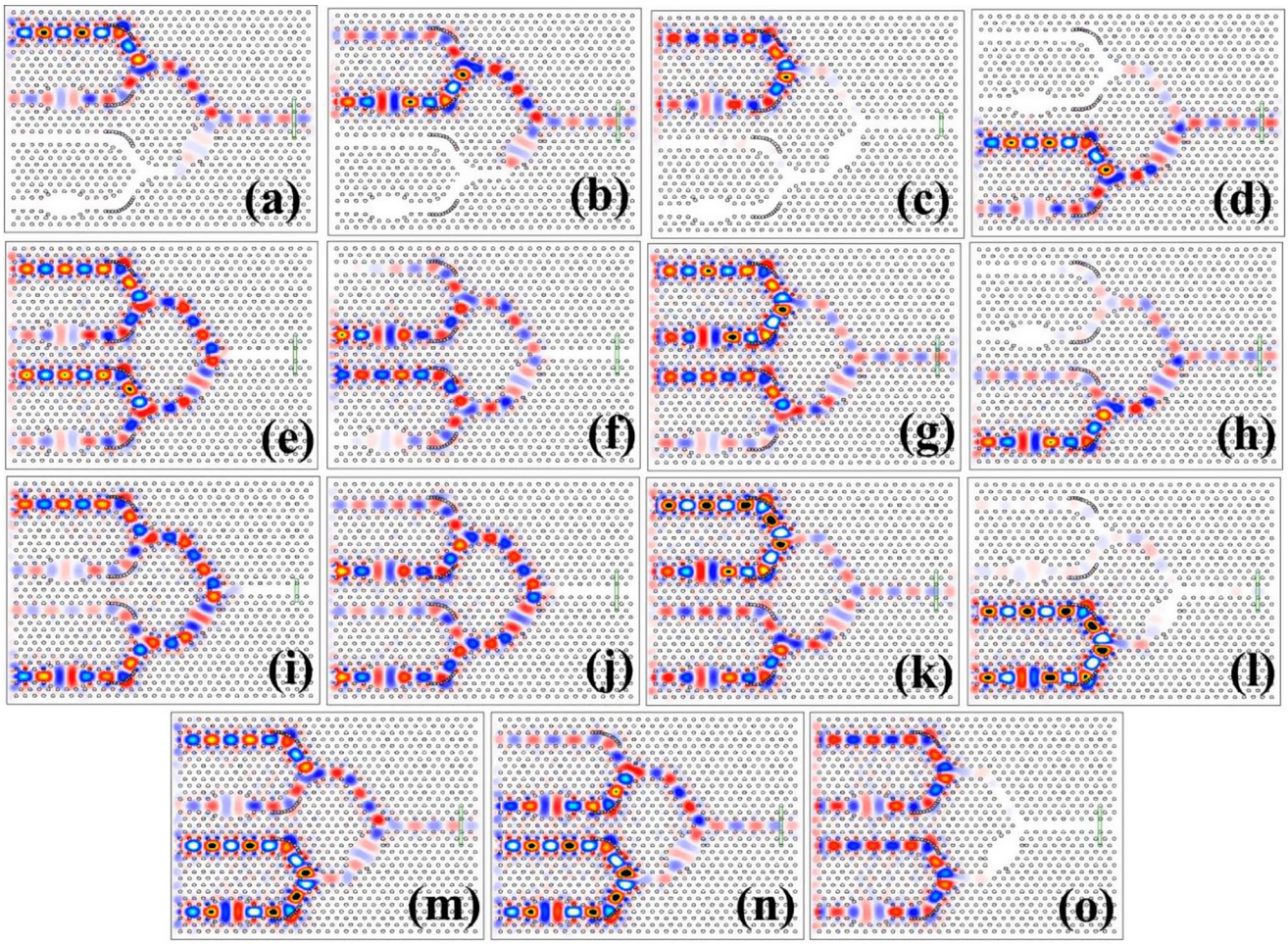

Fig. 7 3-D FDTD propagation profile for the input (ABCD) logic combination of (**a**) 0001 (**b**) 0010 (**c**) 0011 (**d**) 0100 (**e**) 0101 (**f**) 0110 (**g**) 0111 (**h**) 1000 (**i**) 1001 (**j**) 1010 (**k**) 1011 (**l**) 1100 (**m**) 1101 (**n**) 1110 (**o**) 1111

- Definition of the design (PhC structures) using e-beam lithography followed by development and lift-off.
- To design rods etching of the structures is done using RIE (Reactive Ion Etching)/DRIE (Deep reactive-ion etching) method.
- Finally, resist ashing and cleaning the structure.

Moreover, the proposed device is designed based on the simple waveguide structure where no microcavity and microring resonators have been used by changing the physical parameters of the silicon rods. Furthermore, a large band gap is obtained in the range of 1360 nm and 1740 nm where the operating wavelength (1550 nm) falls exactly at the middle of the photonic band gap. However, for fabrication imperfections, the change in the radius of the rods or lattice constant of the structure affects the band characteristics of the structure. Owing to its large photonic bandgap, this change can't affect the electric field propagation characteristics of the proposed device.

Moreover, a 3-dimensional (3-D) FDTD algorithm has been applied to observe the electric field propagation characteristics on a finite height of the proposed device. First of all, a finite height of 1 micrometre of the device is taken where simulation has taken place and all the input possible combinations have been analysed as shown in Fig. 7. From Fig. 7, it is observed that the proposed device shows its behaviour like its 2-D structure.

Various losses in the proposed device

Mainly the proposed device suffers from propagation loss. The loss in the proposed device can be categorized into three major clusters – absorption, radiation, and scattering. The absorption loss originates from the resonance spectra of the base material and the impurities present in the PC devices. The resonance of these impurities also contributes to the absorption loss. On the other hand, radiation loss, especially for the Eigen frequencies that have modes above the light-line, is more prominent in PC slab structures. The modes

in a finite-height 2D slab PC line-defect waveguide are restricted in-plane by the band-gap of the PC The vertical confinement depends on the wave-vector of the band-gap guided modes. An in-plane band-gap guided mode becomes also confined vertically if its wave vector lies below the light-line of the PC. Otherwise, these modes are called radiative modes and they quickly lose their energy along their propagation. Nevertheless, apart from the absorption and radiation loss, the most dominant loss mechanism in an optical mode of PC-based devices is the scattering loss. There are two different types of scattering loss mechanisms are there namely – volume scattering loss and surface scattering loss. The volume scattering loss is exhibited when there are imperfections in the wave-propagating medium. However, the surface scattering loss in a PC slab waveguide becomes dominant and is the most crucial factor behind the belief that PC waveguides usually exhibit higher loss than that of a strip waveguide. The surface scattering loss increases with the increased roughness of PC atoms, which originates during the fabrication process. This surface scattering loss hinders heavily the propagation of higher-order modes as they interact strongly with the waveguide boundaries. Apart from the various losses the proposed structure is considered as a crucial component for future photonic integrated circuits. Moreover, the all-optical 4-input XOR gate can be used in the logic circuits of optical computing like multiplexers, adders, subtractors, etc. The optical XOR gate can also be used in error detection and correction circuits, and data encryption systems. For optical network switching, signal regeneration, and quantum computing optical XOR gate is essential.

Conclusion

In this work, a compact all-optical XOR logic gate with four inputs is proposed using a 2D photonic crystal (PC) design based on rods in air, occupying a minimal footprint of 340 μm². The design leverages light beam interference, eliminating the need for non-linear materials. To maintain symmetry, three Π-phase shifters are integrated into the waveguides, ensuring the required Π-phase difference between optical waves at the junction for destructive and constructive interference. Photonic band gap and projected band analysis have been performed using the plane wave expansion method. Performance metrics have been evaluated using the Finite-Difference Time-Domain (FDTD) algorithm, revealing a high ON-OFF contrast ratio of 14.84 dB at the output port. Even in the worst-case scenario, the device exhibits a response time of 0.57 picoseconds and a bit rate of 660 Gbps. Due to its compact size, low power consumption, high contrast ratio, and high data rate, the proposed XOR gate shows promise for use in optical signal processing devices and photonic integrated circuits.

Acknowledgements Not applicable.

Author contributions Haraprasad Mondal, Kalyan Kumar Ghosh, Himanshu Ranjan Das, Bhargabjyoti Saikia, Mohammad Soroosh, Eshan Adibnia have equally contributed toward designing the devices, simulating the structures, preparing pictures, graphs, and manuscript. All the authors have read and approved the final manuscript.

Funding The authors did not receive funds from any organization for the submitted work.

Data availability We don't have any supplementary dataset along with the manuscript.

Declarations

Ethical approval We declare that the manuscript entitled "Design and Numerical Analysis of 4-Inputs All-Optical XOR Gate in Optical Waveguides" is original, has not been fully or partly published before, and is not currently being considered for publication elsewhere. Moreover, We, further confirm that the order of authors listed in the manuscript has been approved by all of us.

Consent to participate Not applicable.

Consent for publication Not applicable.

Competing interests The authors have no competing interests to declare that are relevant to the content of this article.

References

1. M. Mohammadi, M. Soroosh, A. Farmani, S. Ajabi, Engineered FWHM enhancement in plasmonic nanoresonators for multiplexer/demultiplexer in visible and NIR range. Optik. **274**, 170583 (2023)
2. Z. Salehnezhad, M. Soroosh, H. Mondal, A highly sensitive Plasmonic Graphene-based structure for deoxyribonucleic acid detection. Photonics. **11**, 549 (2024). https://doi.org/10.3390/photonics11060549
3. Y. Taga, Recent progress of optical thin films in the automobile industry. Appl. Opt. **32**, 5519–5530 (1993)
4. T. Kibler, S. Poferl, G. Böck, H.-P. Huber, E. Zeeb, Optical data buses for Automotive Applications. J. Lightwave Technol. **22**, 2184 (2004)
5. J.S. Jaffe, Underwater optical imaging: the past, the Present, and the prospects. IEEE J. Ocean. Eng. **40**, 683–700 (2015). https://doi.org/10.1109/JOE.2014.2350751
6. J.H. Richter, H.G. Hughes, Marine atmospheric effects on electro-optical systems performance. Opt. Eng. **30** (1991). https://doi.org/10.1117/12.55981
7. H. Cheng, C. Xu, X. Jing, H.-Y. Tam, Design of compact LED free-form optical system for aeronautical illumination. Appl. Opt. **54**, 7632–7639 (2015)
8. L. Xu, S. Zhao, T. Wang, Research of line-of-sight angle on aero-optic imaging deviation for vehicles flying at 40–60 km. Opto-electron. Lett. **19**, 242–247 (2023). https://doi.org/10.1007/s11801-023-2123-0

9. K. Goswami, H. Mondal, M. Sen, Optimized design of multiple bends for maximum power transfer in optical waveguide. Optik. **265**, 169448 (2022)
10. S. Khani, A. Farmani, A. Mir, Reconfigurable and scalable 2,4- and 6-channel plasmonics demultiplexer utilizing symmetrical rectangular resonators containing silver nano-rod defects with FDTD method. Sci. Rep. **11**, 13628 (2021)
11. F. Pakrai, M. Soroosh, J. Ganji, A novel proposal for an all-optical combined half adder/subtractor. Opt. Quant. Electron. **54**, 518 (2022). https://doi.org/10.1007/s11082-022-03898-z
12. M. Mansuri, A. Mir, A. Farmani, A tunable nonlinear plasmonic multiplexer/demultiplexer device based on nanoscale ring resonators. Photon Netw. Commun. **42**, 209–218 (2021). https://doi.org/10.1007/s11107-021-00953-9
13. H.P. Mondal, M. Sen, K. Goswami, Design and analysis of all-optical 1-to-2-line decoder based on linear photonic crystal. IET Optoelectron. **13**, 191–195 (2019)
14. R.J. Runser, D. Zhou, C. Coldwell et al., Interferometric ultrafast SOA-based optical switches: from devices to applications. Opt. Quant. Electron. **33**, 841–874 (2001). https://doi.org/10.1023/A:1017553819079
15. H.R. Das, H. Mondal, Investigation of plasmonic material-based T-shaped high extinction ratio electro-absorption modulator with different dielectric materials. Optik. **313**, 171985 (2024)
16. A. Farmani, M. Miri, M.H. Sheikhi, Tunable resonant Goos–Hänchen and Imbert–Fedorov shifts in total reflection of terahertz beams from graphene plasmonic metasurfaces. J. Opt. Soc. Am. B **34**, 1097–1106 (2017)
17. A. Farmani, A. Mir, Z. Sharifpour, Broadly tunable and bidirectional terahertz graphene plasmonic switch based on enhanced Goos-Hänchen effect. Appl. Surf. Sci. **453**, 358–364 (2018)
18. A. Farmani, A. Zarifkar, M.H. Sheikhi, M. Miri, Design of a tunable graphene plasmonic-on-white graphene switch at infrared range. Superlattices Microstruct. **112**, 404–414 (2017)
19. J. Hansryd, P.A. Andrekson, M. Westlund, J. Li, P.-O. Hedekvist, Fiber-based optical parametric amplifiers and their applications. IEEE J. Sel. Top. Quantum Electron. **8**, 506–520 (2002). https://doi.org/10.1109/JSTQE.2002.1016354
20. K. Goswami, H. Mondal, M. Sen, A. Sharma, Design and analysis of AllOptical Isolator based on Linear Photonic crystal. Braz J. Phys. **52**, 78 (2022)
21. C. Prakash, M. Sen, H. Mondal, K. Goswami, Design and optimization of a TE pass polarization filter based on a slotted photonic crystal waveguide. J. Opt. Soc. Am. B **35**(8), 1791–1798 (2018)
22. J.D. Joannopoulos, S.G. Johnson, J.N. Winn, R.D. Meade, *Photonic Crystals: Molding the Flow of Light*, 2nd edn. (Princeton Univ. Press, 2008)
23. F. Mehdizadeh, M. Soroosh, H.A. Banaei, A novel proposal for optical decoder switch based on photonic crystal ring resonators. Opt. Quantum Electron. **48**(20), (2016)
24. F. Parandin, A. Sheykhian, Design and simulation of a 2 × 1 all-optical multiplexer based on photonic crystals. Opt. Laser Technol. **151**, 108021 (2022)
25. M. Abdollahi, F. Parandin, A novel structure for realization of an all-optical, one-bit half-adder based on 2D photonic crystals. J. Comput. Electron. **18**, 1416–1422 (2019). https://doi.org/10.1007/s10825-019-01392-6
26. F. Parandin, R. Kamarian, M. Jomour, A novel design of all-optical half-subtractor using a square lattice photonic crystal. Opt. Quantum Electron. **53**, 114 (2021). https://doi.org/10.1007/s11082-021-02772-8
27. H.P. Mondal, M. Sen, C. Prakash, K. Goswami, C. Sarma, Impedance matching theory to design all-optical AND gate. IET Optoelectron. **12**(4), (2018)
28. A. Farmani, A. Mir, M. Irannejad, 2D-FDTD simulation of ultra-compact multifunctional logic gates with nonlinear photonic crystal. J. Opt. Soc. Am. B **36**, 811–818 (2019)
29. S. Swarnakar, S. Rathi, S. Kumar, Design of all-optical XOR gate based on photonic crystal ring resonator. J. Opt. Commun. **41**(1), 51–56 (2020)
30. A. Mohebzadeh-Bahabady, S. Olyaee, All-optical NOT and XOR logic gates using photonic crystal nano-resonator and based on an interference effect. IET Optoelectron. **12**, 191–195 (2018). https://doi.org/10.1049/iet-opt.2017.0174
31. S.E. Kordi, R. Yousefi, S.S. Ghoreishi et al., All-optical OR, NOT and XOR gates based on linear photonic crystal with high port-to-port isolation. Appl. Phys. B **126**, 169 (2020). https://doi.org/10.1007/s00340-020-07524-2
32. D.G.S. Rao, S. Swarnakar, V. Palacharla et al., Design of all-optical AND, OR, and XOR logic gates using photonic crystals for switching applications. Photon Netw. Commun. **41**, 109–118 (2021). https://doi.org/10.1007/s11107-020-00916-6
33. K. Elhachemi, N. Rafah, A novel proposal based on 2D linear resonant cavity photonic crystals for all-optical NOT, XOR and XNOR logic gates. J. Opt. Commun. **44**, s283–s291 (2023). https://doi.org/10.1515/joc-2020-0184
34. E.G. Anagha, R.K. Jeyachitra, Optimized design of an all-optical XOR gate with high contrast ratio and ultra-compact dimensions. Appl. Phys. B **128**, 21 (2022). https://doi.org/10.1007/s00340-021-07747-x
35. F. Parandin, A. Mohamadi, Design and optimization of a Photonic Crystal-based all-Optical XOR Gate using machine learning. Majlesi J. Electr. Eng. **18**(1), 1–8 (2024)
36. K. Shreya, E.H. Shaik, V.R. Balaji et al., PhC structure for high contrast XOR/OR/NOT logic. Opt. Quantum Electron. **56**, 854 (2024). https://doi.org/10.1007/s11082-024-06748-2
37. R. Rigi, H. Sharifi, K. Navi, Configurable all-optical photonic crystal XOR/AND and XNOR/NAND logic gates. Opt. Quantum Electron. **52**, 339 (2020). https://doi.org/10.1007/s11082-020-02454-x
38. H. Mondal, N. Dutta, M.M. Das et al., Design and simulation of phase shifter based on multimode interference in photonic crystal waveguide. Eur. Phys. J. D **77**, 188 (2023). https://doi.org/10.1140/epjd/s10053-023-00768-5
39. C. Jamois, R.B. Wehrspohn, L.C. Andreani, C. Hermann, O. Hess, U. Gosele, Silicon-based two-dimensional photonic crystal waveguides. Photon Nanostruct. **1**, 1–13 (2003)
40. S.G. Johnson, J.D. Joannopoulos, Block-iterative frequency domain methods for Maxwell's equations in a plane wave basis. Opt. Expr. **8**, 173–190 (2001)
41. P. Bienstman, S. Assefa, S.G. Johnson, J.D. Joannopoulos, G.S. Petrich, L.A. Kolodziejski, Taper structures for coupling into photonic crystal slab waveguides. J. Opt. Soc. Am. B **20**(9), 1817–1821 (2003)
42. S. Assefa, P.T. Rakich, P. Bienstman, S.G. Johnson, G.S. Petrich, J.D. Joannopoulos, L.A. Kolodziejski, E.P. Ippen, H.I. Smith, Guiding 1.5 μm light in photonic crystals based on dielectric rods. Appl. Phys. Lett. **85**(25) (2004)
43. T.M. Shih, A. Kurs, M. Dahlem, G. Petrich, M. Soljačić, E. Ippen, L. Kolodziejski, K. Hall, M. Kesler, Super-collimation in photonic crystals composed of silicon rods. Appl. Phys. Lett. **93**(13) (2008)
44. A.A.M. Kok, C.M. Heesch, E.J. Geluk, M.J.H. Sander-Jochem, J.J.G.M. van der Tol, Y.S. Oei, M.K. Smit, Two-dimensional photonic crystals based on InP rods. Proc. CNM Res. Day, Eindhoven (2006)